Journal of Power Sources 210 (2012) 178–183

Contents lists available at SciVerse ScienceDirect

Journal of Power Sources

journal homepage: www.elsevier.com/locate/jpowsour

Short communication

The thermomechanical stability of micro-solid oxide fuel cells fabricated on anodized aluminum oxide membranes

Chang-Woo Kwon [a], Jae-Il Lee [a], Ki-Bum Kim [a,*], Hae-Weon Lee [b], Jong-Ho Lee [b], Ji-Won Son [b,**]

[a] Department of Materials Science and Engineering, Seoul National University, Gwanak-ro 1, Gwanak-gu, Seoul 151-742, Republic of Korea
[b] High-Temperature Energy Materials Research Center, Korea Institute of Science and Technology, Hwarangno 14-gil 5, Seongbuk-gu, Seoul 130-791, Republic of Korea

ARTICLE INFO

Article history:
Received 3 February 2012
Received in revised form 7 March 2012
Accepted 10 March 2012
Available online 21 March 2012

Keywords:
Micro-solid oxide fuel cell
Freestanding membrane
Anodized aluminum oxide
Platinum electrode
Thermomechanical stability

ABSTRACT

The thermomechanical stability of micro-solid oxide fuel cells (micro-SOFCs) fabricated on an anodized aluminum oxide (AAO) membrane template is investigated. The full structure consists of the following layers: AAO membrane (600 nm)/Pt anode/YSZ electrolyte (900 nm)/porous Pt cathode. The utilization of a 600-nm-thick AAO membrane significantly improves the thermomechanical stability due to its well-known honeycomb-shaped nanopore structure. Moreover, the Pt anode layer deposited in between the AAO membrane and the YSZ electrolyte preserves its integrity in terms of maintaining the triple-phase boundary (TPB) and electrical conductivity during high-temperature operation. Both of these results guarantee thermomechanical stability of the micro-SOFC and extend the cell lifetime, which is one of the most critical issues in the fabrication of freestanding membrane-type micro-SOFCs.

1. Introduction

During the past decade, micro-solid oxide fuel cells (micro-SOFCs) based on backside-etched freestanding membrane designs were extensively studied for application in alternative high-efficiency portable power sources [1–6]. Because the deposition of electrolyte layers over dense substrates followed by backside etching of the substrates is the most straightforward method to obtain ultra-thin and gas-impermeable electrolytes for SOFCs that operate at lower temperatures, most researchers adopted this process sequence without much alteration. Nevertheless, micro-SOFCs of this freestanding electrolyte membrane design have significant issues in terms of their thermomechanical reliability and stability [2]. The main origins of the limitations are the thermomechanical vulnerability of the electrolyte membrane and the fast degradation of nanoporous noble metal electrodes, even in the low operation temperature regime of SOFCs ($\leq$500 °C) [7,8]. Undoubtedly, employing porous supporting structures for the electrolyte membrane can mitigate the above-mentioned problems. Nonetheless, there are several issues to consider in the selection of suitable porous supporting materials in terms of the optimum pore size, the optimum pore density, and the continuity of the pore through the supporting material. The thermal stability of this material in conjunction with the electrolyte can be another issue to consider. More importantly, it is often observed that micro-SOFCs fabricated on porous substrates show much lower open-circuit voltages (OCVs) [9,10].

Previously, authors have reported the successful realization of a freestanding membrane micro-SOFC supported by a porous anodic aluminum oxide (AAO) membrane with a thickness of approximately 600 nm [1]. Utilization of an AAO membrane is a natural choice for the porous substrate due to its relatively easy fabrication process and the easy controllability of the pore size from a few tens of nanometers down to a few nanometers and a pore density of more than 10^{11} cm^{-2}. Pore continuity is guaranteed due to the intrinsic nature of the pore formation. Moreover, the honeycomb structure of the nanopores guarantees the mechanical stability of the overall structure.

Before this study, the realization of micro-SOFCs on porous supports was largely unsuccessful, especially in terms of the low OCVs obtained because of the difficulty of depositing a gas-impermeable electrolyte over porous supports [2,9,10]. In the previous report, the origin of these low OCVs was determined to be the pinhole formation that was caused by the selective nucleation and growth of electrolytes during pulsed laser deposition (PLD); this problem was alleviated by blocking the pinholes using a conformal deposition of thin films using atomic layer deposition (ALD). As a result, high OCVs and high performance of the micro-SOFC were successfully achieved [1]. The thermomechanical stability of the micro-SOFC fabricated with this scheme, however, was not investigated. In this manuscript, the excellent thermomechanical stability of the micro-SOFC thus fabricated will be discussed.

* Corresponding author. Tel.: +82 2 880 7095; fax: +82 2 885 5820.
** Corresponding author. Tel.: +82 2 958 5530; fax: +82 2 958 5529.
E-mail addresses: kibum@snu.ac.kr (K.-B. Kim), jwson@kist.re.kr (J.-W. Son).

0378-7753/$ – see front matter © 2012 Elsevier B.V. All rights reserved.
doi:10.1016/j.jpowsour.2012.03.020

2. Experimental

The thermomechanical stability of the micro-SOFC will be discussed in terms of two separate issues. First, the stability of the Pt electrodes, both the anode and the cathode, will be discussed. Then the structural integrity of the AAO membrane will be investigated.

2.1. Thermal stability of Pt electrodes over an AAO template

To avoid other sources of failure from using a freestanding AAO membrane, commercial AAO disks were used as a supporting material for the investigation. Commercial AAO disks (Anodisc, Whatman, Inc.) with 100 nm pores were used to test the stability of the Pt electrodes. For comparison, porous Pt electrodes were also deposited on a 500-nm-thick YSZ/1-μm-thick thermal SiO_2/Si substrate. The Pt electrode on top of the AAO substrate was deposited at a 0.67 Pa Ar pressure and at a 70 W power, while the Pt electrode on top of the YSZ layer was deposited at a high Ar pressure of 10 Pa and at a power of 70 W to obtain a porous Pt layer. Both of the films were deposited at room temperature. It is important to note that the Pt sputtering condition is different in these two cases. This difference is unavoidable to secure gas–electrode–electrolyte triple phase boundaries (TPBs) because two different types of substrates are used: one is a porous substrate, and the other one is a planar substrate. On the porous substrate, a TPB is easily formed even with dense Pt because the pores already exist on the deposition surface. On the planar substrate, the pores should be introduced to the Pt layer itself by depositing the layer at a high ambient pressure.

The microstructural change of Pt electrodes was investigated after a 2 h annealing process at the temperature of 400–700 °C with scanning electron microscopy (SEM). Moreover, the structural degradation was evaluated by the electrical resistance change of the electrode as a function of the dwell time at an elevated temperature of 600 °C. To do this, two electrode contacts (Ti 50 nm/Pt 300 nm) that were separated by 7 mm from each other were deposited on YSZ and AAO substrates, and Pt was subsequently deposited over the two separated contacts.

2.2. Mechanical stability of AAO-supported membranes

To compare the mechanical stability of AAO-supported electrolyte membranes with that of a freestanding membrane, square-shaped membranes with lateral dimensions of 50–1200 μm were fabricated. As shown in Fig. 1, the test die contained three membranes of each size. Double-side polished 300-μm-thick silicon wafers were used to fabricate freestanding silicon nitride membranes, and 500-nm-thick silicon nitride was deposited by low-pressure chemical vapor deposition (LPCVD) on both sides of the silicon wafer as an etch mask. Then the backside silicon nitride layer was photolithographically defined and removed by reactive ion etching (RIE). The exposed silicon areas were wet etched with a 30% KOH solution at 80 °C. For the fabrication of the AAO membrane, an additional 600-nm-thick AAO layer with a 40 nm average pore size was fabricated on the silicon nitride membrane. The detailed experimental procedure used to form the AAO membrane structure was described in a previous article [1]. On top of these two different structures, 500-nm and 1-μm-thick YSZ electrolyte layers were deposited by PLD at an elevated temperature of 500 °C. After the deposition, the fraction of surviving membranes without breakage was observed by means of an optical microscope.

2.3. Stability test of the AAO-supported micro-SOFC as a function of dwell time

Finally, to test the longevity of the AAO-supported micro-SOFC, a Pt anode layer was first sputter-deposited at an Ar pressure of 0.67 Pa and at a sputtering power of 70 W over the AAO membrane. Then a YSZ electrolyte layer with a total thickness of 900 nm was deposited in two steps of 450 nm each by PLD at 300 °C with a laser fluence of 2.5 J cm^{-2}, and a thin Al_2O_3 intermittent layer was deposited by ALD in between the 450-nm-thick YSZ electrolyte layers. Lastly, 80-nm-thick porous Pt cathode layers (10 Pa Ar pressure and 25 W sputtering power) were sputter-deposited on the YSZ layer. Again, the detailed steps of the device fabrication were reported in our previous publication [1]. Freestanding micro-SOFCs with the same 900-nm-thick YSZ electrolyte layer were also fabricated to compare the stability as a function of dwell time. A YSZ electrolyte was also deposited at 300 °C over the silicon nitride membrane by PLD; the nitride layer was removed by RIE afterwards. Then 80-nm-thick porous Pt films (10 Pa Ar pressure and 25 W sputtering power) were deposited on both sides of the YSZ electrolyte as a cathode and an anode.

The longevity test was performed at 400 °C as a function of time. 4% H_2 (N_2 balance) was used as the fuel and the flow rate was 25 sccm. The cathode side was exposed to free-flowing air. The cells were held at 400 °C, and both the OCV and the cell output at 0.8 V were measured at an interval of 1 h using a potentio/galvanostat (Solartron 1287).

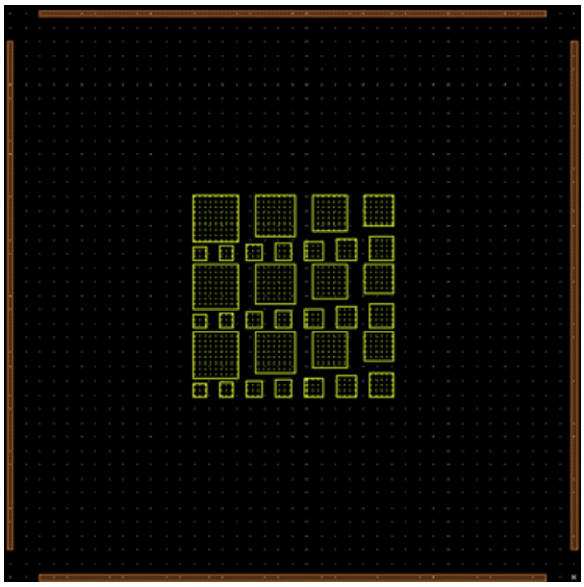

Fig. 1. Layout of the membrane stability test die containing square membranes with lateral dimensions of 50–1200 μm.

3. Results and discussion

3.1. Thermal stability of Pt electrodes

Until now, while there have been many efforts to develop thermally stable electrode materials [11–13], Pt has been known as one of the most commonly utilized electrode materials due to its catalytic effect and low electrical resistance. Because the electrode material should have a large TPB length of the gas–electrode–electrolyte, the electrode should be deposited to have enough porosity and still be electrically connected to harvest electrons. Moreover, the micro-SOFC should operate at a relatively high temperature to reduce the ohmic loss of electrolytes. Naturally, this high-temperature operation will result in the degradation of the electrode material, most notably in the agglomeration of the porous Pt electrode.

Fig. 2 shows the SEM images of as-deposited and annealed Pt electrodes on YSZ and AAO substrates. The Pt electrode was

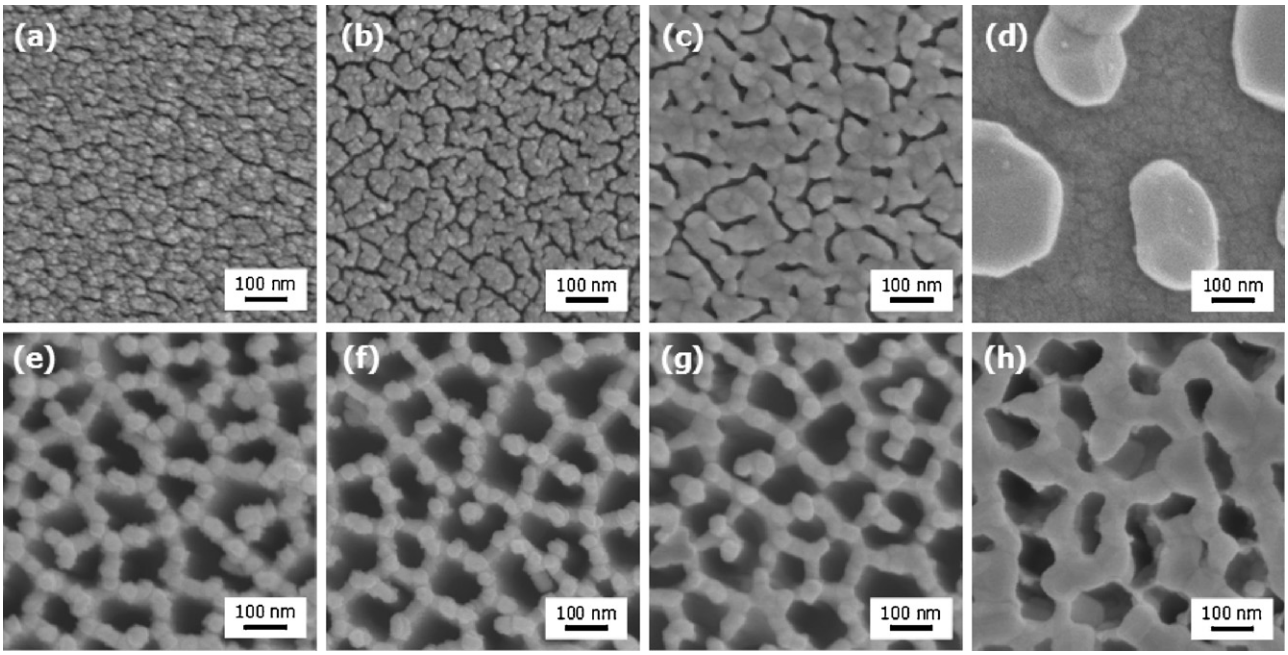

Fig. 2. SEM images of porous Pt deposited on YSZ ((a)–(d)) and AAO substrates ((e)–(h)). As-deposited ((a) and (e)) and annealed in air for 2 h at the elevated temperatures of 400 °C ((b) and (f)), 500 °C ((c) and (g)), and 600 °C ((d) and (h)).

annealed at temperatures ranging from 400 °C to 600 °C in air. Again, it should be noted that a dense Pt layer was deposited on top of AAO, while a porous Pt layer was deposited on top of the YSZ substrate. The as-deposited 80-nm-thick Pt electrode on YSZ exhibited a nanoporous microstructure with an average pore size of 5–20 nm (Fig. 2(a)). After annealing at 400 °C, the Pt film begins to agglomerate (Fig. 2(b)), and the clusters grow with increasing temperature. The fine pores are interconnected with each other, and fewer, larger pores with sizes of 100–200 nm appear as a result of the 500 °C annealing (Fig. 2(c)). Eventually, the Pt clusters are isolated, and electrical connections between the clusters are lost across the entire substrate at 600 °C (Fig. 2(d)). Undoubtedly, one can notice that degradation of the Pt electrode occurs, and it will severely affect the functionality of the device due to the variation of the TPB length and because of the loss of the electrical connectivity during the high-temperature operation.

On the contrary, metal coalescence and significant changes in pore size are not observed in the Pt layer deposited on top of the AAO substrate at annealing temperatures up to 500 °C (Fig. 2(e)–(g)). After annealing at 600 °C, Pt clusters begin to grow, and this reduces the average pore sizes. The Pt clusters, however, still appear to be interconnected with each other, creating good electrical connectivity.

In the case of metal electrodes serving only as electronic conductors, the TPB where the electrochemical reaction takes place would be formed two-dimensionally along the boundary lines of clusters. Therefore, it is important that the porous film contains a large number of fine pores and that this fine structure be maintained over time for better performance of the cells. Thus, the TPB length was evaluated with image analyzing software GAIA Blue v.5.2.2.0 (Mirero Inc.). SEM images are converted to binary images with a proper contrast adjusting process (Fig. 3(a)), and then the pixels of cluster boundaries are counted. Fig. 3(b) shows the change in the TPB length of annealed clusters with the ratio of the initial TPB length of the as-deposited clusters as a function of temperature. As shown in Fig. 3(b), the TPB length of porous Pt electrodes on the YSZ substrate gradually decreases with temperature, and only approximately 30% of the TPB remains after annealing at 500 °C. In contrast, the TPB in the Pt on AAO is maintained with a small decrease of length at 500 °C, and approximately 70% of the TPB remains, even after annealing at 600 °C.

Furthermore, the improved thermal stability of the AAO-supported electrode structure can be seen more clearly in the electrical conductance changes as a function of time. The Pt electrodes on the YSZ and AAO substrates were fabricated for the electrical conductance change measurement, and the tested specimens formed over the AAO disks are shown in Fig. 4. It should be noted that the resistance changes in the contact pads are negligible during the experiment, which is confirmed by measuring the sheet resistance change of the contact pads before and after annealing. Therefore, it can be assumed that the observed electrical conductance change mostly originates from the structural degradation of the Pt electrodes over each substrate. As can be seen in Fig. 5, the conductance of porous Pt on the YSZ substrate drastically decreases with time, and only 10% of the initial conductance is obtained after 5 h. In contrast, the conductance of Pt on AAO was decreased by only 20% of the initial value, even after 5 h of annealing.

The driving force of coarsening is minimization of the free energy of the system associated with the interfaces. The difference in the degree of the coarsening behavior between the Pt electrode on YSZ and AAO substrates can be ascribed to the difference in the initial film density and the surface area. To obtain a large TPB length, a film with a low density should be deposited by increasing the Ar pressure during the Pt sputtering on the YSZ substrate. In the case of the electrode on the AAO substrate, however, a high-density film can be used to make a porous electrode, owing to the inherent porous nature of the AAO substrate. The nanoporous Pt electrode possesses a significantly larger surface area inside the film, and this works as a high driving force for the agglomeration at high temperatures. Moreover, for the real cell structure, the YSZ electrolyte layer is deposited on top of the Pt anode layer, which results in a sandwiched electrode structure in the AAO-supported cell (Fig. 4(b)). It is easily expected that this structure will promote the stability of the Pt anode layer. Indeed, the solid circles in Fig. 5 indicate that the electrical conductance of the Pt electrode sandwiched between the bottom AAO substrate and the upper YSZ layer

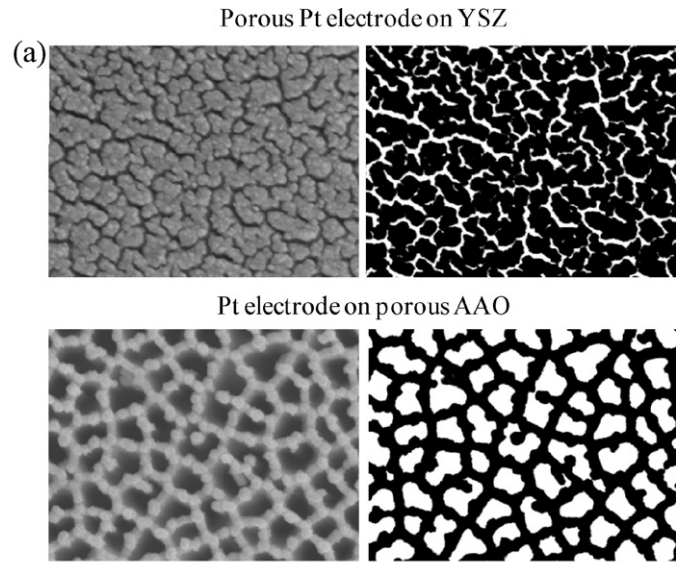

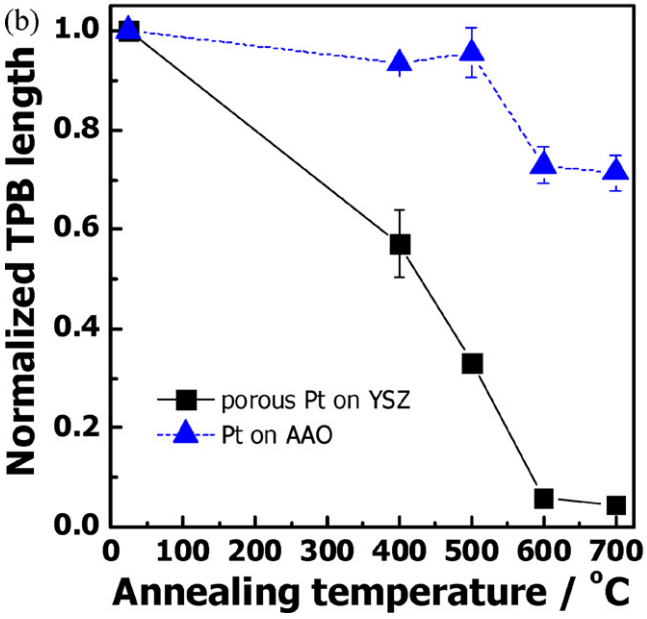

Fig. 3. (a) SEM images and converted binary images of porous Pt deposited on YSZ and AAO substrates and (b) the change of the normalized TBP length of Pt electrodes on YSZ and AAO substrates as a function of temperature.

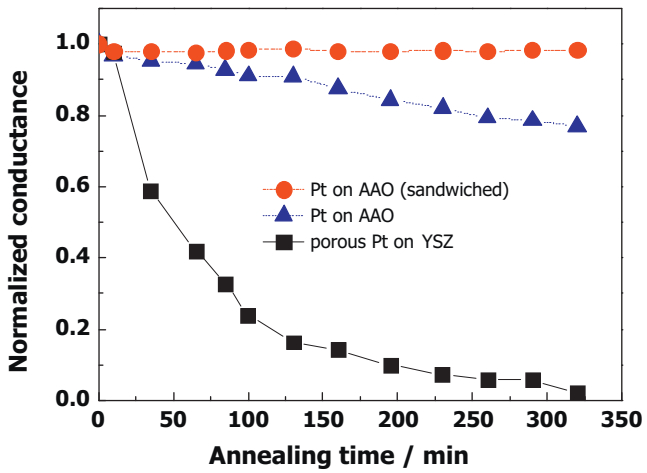

Fig. 5. The change of the normalized conductance of Pt electrodes on YSZ and AAO substrates as a function of time at 600 °C.

is well preserved at the same level, even after annealing at 600 °C over 5 h.

3.2. Mechanical stability of AAO-supported membranes

Fig. 6 shows the fraction of surviving freestanding membranes (yield) after deposition of the YSZ electrolyte with and without an AAO layer. In the case of the YSZ/silicon nitride membrane, the yield decreases as the membrane dimension increases. As shown in Fig. 6(a), for the samples with a 500-nm-thick YSZ layer, few membranes survive for lateral dimensions of the membrane that were longer than 600 μm. Moreover, no membrane survived for the lateral dimension longer than 150 μm when the thicker YSZ film (1 μm) was deposited. In contrast, all of the membranes with AAO supports survived irrespective of the lateral dimension of the membrane and the thickness of YSZ up to 1 μm (Fig. 6(b)). This clearly indicates that the AAO support significantly improves the mechanical stability of the micro-SOFC device.

In addition, it is noted that the AAO membrane effectively reduces the difference in the thermal expansion coefficient of the components. The thermal expansion coefficients of YSZ, silicon nitride, and alumina are approximately 11, 1.6, and 7.6 × 10^{-6} K^{-1}, respectively [14,15]. The thermal expansion coefficient of AAO lies between that of the YSZ electrolyte and silicon nitride. This result indicates that the device can be made more stable during the thermal cycles of operation and that a larger freestanding membrane area can be achieved in the AAO-supported membrane.

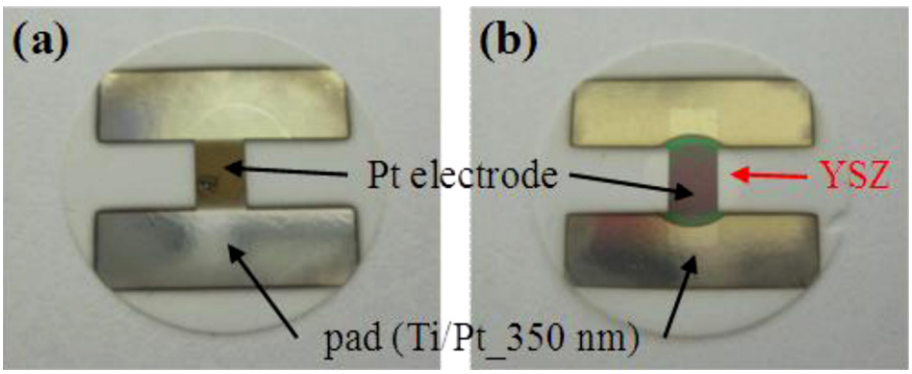

Fig. 4. Porous Pt deposited on AAO membranes (anodisc): (a) without a YSZ top layer and (b) with a YSZ top layer.

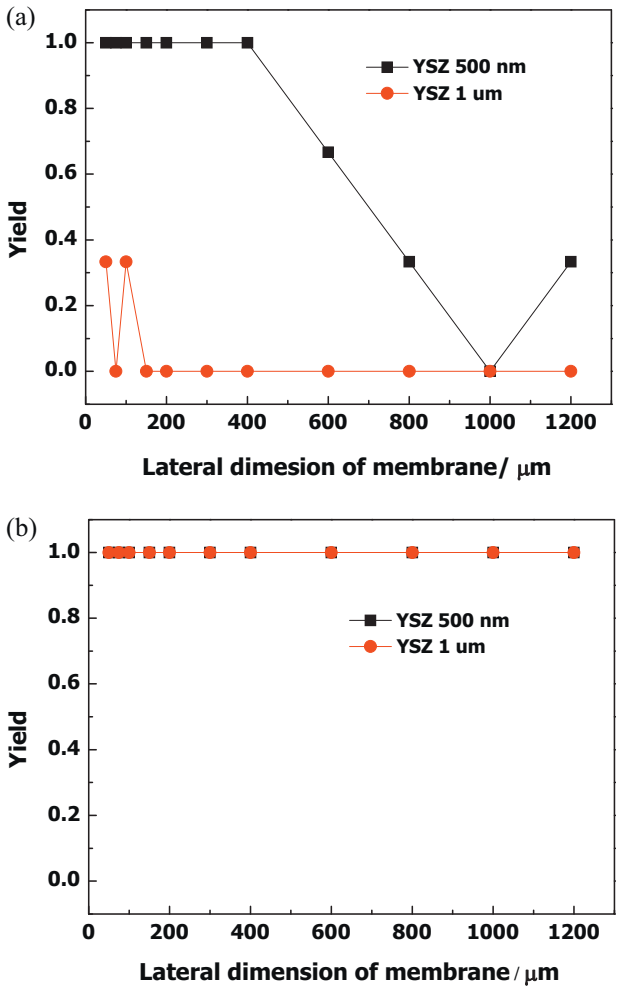

Fig. 6. The fraction of surviving freestanding membranes (yield) after deposition of the YSZ electrolyte at 500 °C: (a) yield of the flat membrane and (b) that of the AAO-supported membrane.

3.3. Longevity of an AAO-supported micro-SOFC

Finally, the prolonged lifetime of the micro-SOFC fabricated as described previously is reported in this section. In Fig. 7, the longevity test result of the AAO-supported micro-SOFC at 400 °C is presented. The OCV of the cell was perfectly retained during the test time, and 90% of the initial power was sustained, even after approximately 17 h (1000 min) of operation. A certain amount of degradation was unavoidable because porous Pt was utilized as a cathode electrode without any structural support. Compared with that of common SOFCs, the degradation of the AAO-supported micro-SOFC is quite substantial. Even so, the degradation rate is much improved in comparison with the freestanding membrane SOFC in our study, as well as with the cell reported elsewhere [5], showing 50% degradation after 12 h of operation at 400 °C. This result clearly demonstrates the suppression of electrode agglomeration with the AAO membrane support. As previously mentioned, using the AAO supporting structure on the anode side would significantly improve the reliability of the freestanding membrane micro-SOFC.

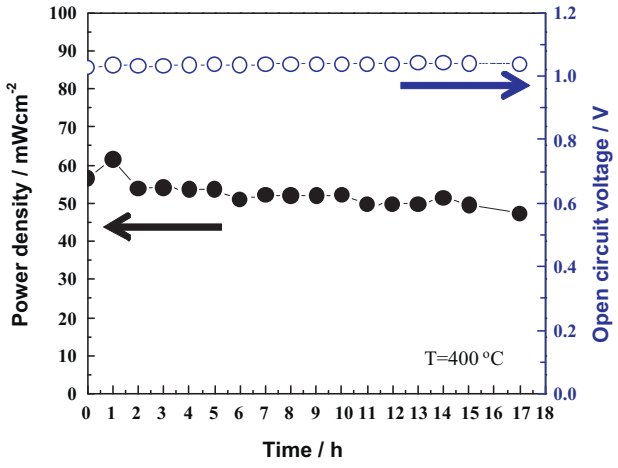

Fig. 7. OCV (open symbols) and power density (close symbols) at 0.8 V of an AAO-supported micro-SOFC as a function of dwell time at 400 °C.

In contrast, all of the flat freestanding membrane SOFCs were broken before 1 h had passed at 400 °C in our study. In comparison with another study [5], the stability of the flat freestanding membrane was worse. This was probably due to the thicker YSZ electrolyte (900 nm) compared with that (~100 nm) of the other report [5]. As can be deduced from the results of Section 3.2, a membrane with a thicker electrolyte has an inferior mechanical stability.

4. Conclusion

The potential for improving the thermomechanical stability of freestanding membrane micro-SOFCs by employing AAO as a structural support is investigated. First, the stability of the microstructural and electrical properties of Pt electrodes is investigated by monitoring the changes in the microstructure and the electrical conductance at the elevated temperatures, and it is shown that the degradation of the sandwiched Pt electrode is significantly mitigated compared with that of the porous Pt electrode that is directly deposited on the electrolyte surface. Second, the mechanical stability of the freestanding membrane is improved by inserting the AAO layer between the electrolyte and silicon nitride membrane. These improvements are expected to provide structural stability to micro-SOFCs when the AAO membrane is used as an electrode support. In fact, as a result, the longevity of the AAO-supported micro-SOFC is considerably improved when compared with that of common, flat, freestanding membrane micro-SOFCs. The present study suggests a possible solution to overcome the thermomechanical frailty of freestanding membrane micro-SOFCs, which is the most fatal issue preventing the practical use of freestanding membrane micro-SOFCs.

Acknowledgements

This work was supported by the Institutional Research Program of the Korea Institute of Science and Technology (KIST) and the Global Frontier Program (2011-0031579) through the National Research Foundation (NRF) grant funded by the Ministry of Education, Science and Technology (MEST), the Republic of Korea. It was also partially supported by the World Class University (WCU) program through the NRF funded by the MEST (R31-2008-000-10075-0).

References

[1] C.-W. Kwon, J.-W. Son, J.-H. Lee, H.-M. Kim, H.-W. Lee, K.-B. Kim, Adv. Funct. Mater. 21 (2011) 1154–1159.
[2] A. Evans, A. Bieberle-Hütter, J.L.M. Rupp, L.J. Gauckler, J. Power Sources 194 (2009) 119–129.
[3] H. Huang, M. Nakamura, P.C. Su, R. Fasching, Y. Saito, F.B. Prinz, J. Electrochem. Soc. 154 (2007) B20–B24.
[4] J.H. Shim, C.C. Chao, H. Huang, F.B. Prinz, Chem. Mater. 19 (2007) 3850–3854.

[5] K. Kerman, B.-K. Lai, S. Ramanathan, J. Power Sources 196 (2011) 2608–2614.
[6] M. Tsuchiya, B.-K. Lai, S. Ramanathan, Nat. Nano 6 (2011) 282–286.
[7] C.D. Baertsch, K.F. Jensen, J.L. Hertz, H.L. Tuller, S.T. Vengallatore, S.M. Spearing, M.A. Schmidt, J. Mater. Res. 19 (2004) 2604–2615.
[8] V.T. Srikar, K.T. Turner, T.Y.A. Ie, S.M. Spearing, J. Power Sources 125 (2004) 62–69.
[9] Y.I. Park, P.C. Su, S.W. Cha, Y. Saito, F.B. Prinz, J. Electrochem. Soc. 153 (2006) A431–A436.
[10] A. Ignatiev, X. Chen, N. Wu, Z. Lu, L. Smith, Dalton Trans. 40 (2008) 5501–5506.
[11] X.H. Wang, H. Huang, T. Holme, X. Tian, F.B. Prinz, J. Power Sources 175 (2008) 75–81.
[12] A.C. Johnson, B. Lai, H. Xiong, S. Ramanathan, J. Power Sources 186 (2009) 252–260.
[13] D.-H. Myung, J. Hwang, J. Hong, H.-W. Lee, B.-K. Kim, J.-H. Lee, J.-W. Son, J. Electrochem. Soc. 158 (2011) B1000–B1006.
[14] F. Tietz, Ionics 5 (1999) 129–139.
[15] T.F. Retajczyk Jr., A.K. Sinha, Thin Solid Films 70 (1980) 241–247.